A MICRO HOT PLATE FOR COMBUSTIBLE GAS SENSING

6.971
Design and Fabrication of Micro-electromechanical Devices

Instructors

Prof. M. Schmidt
Prof. S. Senturia

Team F

Tamara Floyd
Kevin Lohner
David Robinson
Joel Voldman

December 10, 1997

INTRODUCTION

Design Specifications

Our objective was to design a combustible gas sensor which uses a Pt thin film as a catalyst. The design includes a micro-machined thermally-isolated element, which has a very small thermal mass and corresponding low power and fast response time. The micro-machined structure is to be fabricated using a foundry CMOS process and XeF2 silicon etching to release the heater as a post-CMOS, post-packaging process. The Pt thin film will be deposited by chemical vapor deposition after the heater is released. The micro hot plate has separate heater and temperature sensing resistors. The heater resistor is used both to heat the device for Pt chemical vapor deposition, and to heat the device to the operation temperature of the sensor. In operation, the micro hot plate is held at elevated temperature, and the power to maintain this temperature is monitored. A sharp reduction in power supplied by the voltage source is indicative of a catalytic reaction on the Pt, and thus signals the presence of combustible gases. The design parameters are listed in Table 1.

Table 1:Design Parameters

Sensor Operating Temperature	300°C
Sensing Area	100 μm X 100 μm
Thermal Time Constant	1 ms
Minimum Resolvable T change at fixed power	.5 °C
Maximum permitted temperature difference over sensing area	2 °C
Maximum power dissipation	5 mW
Maximum supply voltage	5 V
Micro CVD conditions	
Deposition Temperature	400°C
Deposition Thickness	1000 A
Deposition Rate @ 400°C	5 A/sec
Activation energy for deposition	1.8 eV

Background

Hydrocarbon (HC) sensors have a variety of industrial and consumer applications. Industrially, hydrocarbon sensors are used in research labs for HC monitoring. Industrially, they are used in manufacturing facilities for detecting the hydrocarbon emissions from the stacks. In this application, a particular industry may use and thus emit hydrocarbons. Exposure to hydrocarbons has negative physiological and environmental effects so their emission is federally regulated. Consequently, companies use sensors for stack testing to demonstrate compliance to the EPA emission guidelines. Sensors are also used to test catalytic converters, which are catalysts located between automobile engines and the exhaust pipe to convert harmful gases such as hydrocarbons, carbon monoxide and NO_X to less harmful gases such as H_2O, N_2, and CO_2. In many states, automobile owners must demonstrate that their vehicles meet emission guidelines by having their automobile tested. These tests are performed using chemical sensors. Sensors also may be, and perhaps are, used to monitor or test for gas leaks in homes that use natural gas for heating and or cooking. In short, hydrocarbon sensors may be used in any environment where hydrocarbons are present.

Solid-state sensors are a popular choice for HC chemical sensing. Solid state sensors include semiconductor sensors and solid electrolytes[1]. Broadly, solid state sensors operate based on the response of the solid to its chemical environment. This response may be realized by a change in the solid's electrical properties, such as resistance or piezoelectricity. Additionally, other types of solid-state sensors are based on other principles such as acoustics, optics and thermo-chemistry. [2]

Non-solid-state hydrocarbon sensors include thermal conductivity detectors and flame ionization detectors. They operate based on principles of the sample. For example, the flame ionization detectors (FID) detect the ions that are created as the hydrocarbon reacts and fragments whereas the thermal conductivity detector technology (hot-wire anemometry) uses the knowledge of the thermal conductivity and pressure of the gas to relate heat transfer to the amount of the gas present. In evaluating the various technologies, issues such as cost, reliability, reproducibility, and stability dictate which sensors are used for particular applications. [3]

The Flame Ionization Detector

The FID is currently the technology used most extensively for HC sensing; thus, a comparison is made between the FID and our solid state catalytic semiconductor sensor to identify a market for our semi-conductor sensor.[4] During operation, a gas stream of unknown HC concentration is fed into the sampling tube of the FID. This tube leads into a hydrogen/air flame which surrounds an electrode. The response obtained with the FID varies in proportion to the number of carbon atoms in the molecule. This is observed because the carbon atoms in a HC are quantitatively converted to methane molecules in the lower part of the flame where a flux of the mobile hydrogen atoms is formed by diffusion inward from the combustion zone. The atomic hydrogen first adds to multiple bonds. At slightly higher temperatures carbon-carbon bonds are broken, and eventually all carbons are completely hydrogenated to methane. These processes are extremely fast and come to completion in the flame at 600-650°C, that is at temperatures well below the temperatures found in the combustion zone. Subsequently, the methane molecules are converted to carbocations, positively charged carbonaceous particles, that interact with the electrode to produce a signal which "counts" the carbons. [5,6] The advantage of the FID is that it is reliable, stable and well-developed. The disadvantages are that signals vary with pressure and it is a vacuum system; thus, it is expensive.

Our Semi-conductor Sensor

Alternatively, there is our thermal catalytic semiconductor sensor. The sensor consists of a catalyst, a thin film temperature sensor, a thermally isolated mass to assure fast response and low power consumption, and associated packaging.

During operation, the catalyst accesses a lower operating temperature, and the reactants proceed to react exothermically to generate heat that causes a temperature signal , and then the signal is transduced using the resistivity property of a metal temperature sensor. Metals exhibit the property of increasing resistivity with increasing temperature. Thus, the temperature rise is transduced as a resistance change by passing a constant current through the temperature sensor, measuring the voltage drop, calculating the resistance and determining the temperature, which is a known function of resistance. The disadvantages of the thermal catalytic semiconductor are that they have problems with reproducibility and stability due to processing and packaging variances as well as the fragility of the small suspended components. The advantages are that they have a substantial market because they are inexpensive, relative to other gas sensing means, and they are adequate for many purposes. [7]

CATALYSIS

We use a catalyst to operate at lower temperature and to localize the reaction to the hot plate surface. The reaction is what generates the heat which causes the temperature rise that is transduced. The conversion of a set of reactants to products is governed by the thermodynamic properties of the reactants. Thermodynamically, a system will proceed to its equilibrium, but thermodynamics does not offer information about the speed at which the system will proceed to equilibrium. A reaction has certain pathways available and it will prefer the path that requires the lowest activation energy. This is where kinetics becomes important.

One concept important in the kinetics of chemical reactions is catalysis. A catalyst is a material that speeds a reaction, but is not consumed. It is effective because the material has properties that offer an alternate pathway for the reaction to proceed. The alternate pathway requires less energy for activation and thus proceeds faster at a given temperature when compared to the corresponding uncatalyzed reaction. Combustion is a rapid process so instead of using the catalyst to increase the rate, we kept our rate constant and used the catalyst to access a low temperature operating regime. The combustible gases can react spontaneously without the catalyst at a given temperature, but then the assumption of the transfer of the heat of reaction to the thermally-isolated mass would not be valid so in addition to accessing lower operating temperatures, we also localize the reaction to the surface and simplify our heat transfer model.

One design parameter is to use Pt for our sensor catalyst. Platinum is chosen as the catalyst for this sensor because combustion is an oxidation reaction and platinum is an excellent oxidation catalyst. A good oxidation catalyst it is not easily oxidized and should chemisorb oxygen. Only Ru, Rh, Pd Os, Ir, Pt, Ag and Au are sufficiently resistant to remain unoxidized.[8] Of these, gold has little adsorptivity in general and hence has little catalytic activity. Os and Ir are very scarce. There are other metals from the list available for catalysis, but another constraint is that the metal must be compatible with the clean room environment. Thus Pt is a good choice.

Another design parameter is to use 1000 A of Pt. Platinum is very expensive so we want to limit the film thickness. Catalyticly, there is no advantage to having a thicker film because only the surface Pt is used for catalysis. The limiting factors are film adhesion and agglomeration, the decomposition of a thin continuous film into a collection of beads. [9]

In our design, we used our sensor heater for chemical vapor deposition of the platinum. This is advantageous because we can use the uniform temperature distribution we achieve to deposit our platinum. Platinum deposition follows an Arrhenius temperature dependence shown in Eq. 1. Uniformity is a strong function of temperature so it is very important to have a uniform temperature distribution.

$$-rate = Ae^{\left[\frac{E_a}{RT}\right]} \qquad [1]$$

In general, catalyzed reactions operate at lower temperatures than their corresponding uncatalyzed reactions, so 300°C seems high for our sensor operating temperature. The problem is that although oxygen is strongly adsorbed by metals, apparently, the bonds are generally too strong to be easily arranged, so higher temperatures are generally required for oxidation reactions to occur on metals. Our goal is to operate as close to ambient as possible because we use energy to heat our catalyst to the desired operating temperature, and 300°C represents the optimal temperature.

METHODOLOGY AND TRADE STUDIES

HEATER DESIGN APPROACH

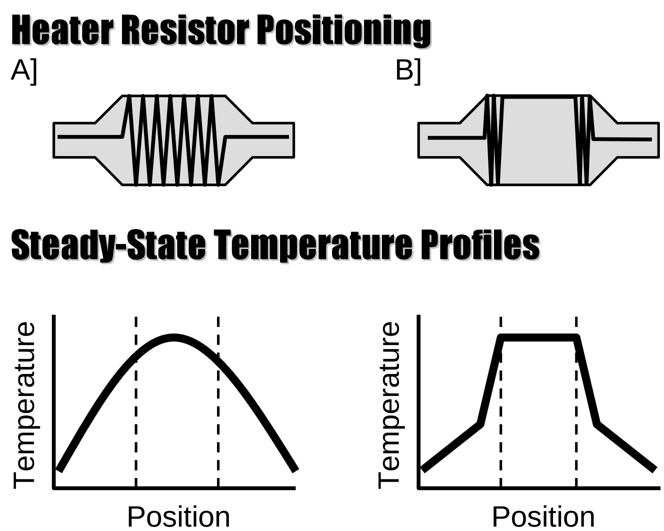

Figure 1: Qualitative steady-state temperature profiles as a function of heater resistor positioning. Case A depicts heat generation across the entire plate surface. Case B depicts heat generation along two sides of the plate. Case B exhibits a more uniform temperature profile across the plate.

The design of the basic hotplate shape and the positioning of the heater resistors are the two most important factors that govern the performance of the micro-hotplate device. Due to structural, performance, and processing concerns (which will be discussed in more detail later in the report), the team decided to construct the heater resistors and temperature sensor resistors on two different poly-silicon layers. This allowed the device to be built with just 2 legs, rather than 4 (as was suggested in the Problem Statement).

The design of the heater resistor layout was also carefully investigated. Figure 1 shows qualitative steady-state temperature profiles as a function of two different heater resistor layouts. Case A shows a standard layout design with heater resistors snaked across the entire sensor plate (as was suggested in the Problem Statement). Because conductive heat flow is governed by the equation,

$$Q=-kA\,(dT/dx) \qquad [2]$$

it stands to reason that if there is heat generation across the plate, Q, there must also be a temperature delta, dT/dx. Initial calculations with this design showed the resultant dT/dx to be on the order of 50°C. This represents too high a variability for suitable performance of the sensor. Upon further review and consultation from Dr. Aleksander Franz of the MIT Chemical Engineering department, the design, as shown in Case B, was investigated. This design, with the heating elements on both sides of the sensor plate, eliminated the Q term across the plate, thus minimizing the undesirable dT/dx term. Accordingly, the Case B configuration was adopted as our project design. This design also lent itself well to simplified, one dimensional heat transfer modeling.

TRADE STUDIES

In deciding on the final structural dimensions of the micro-hotplate, it was important to consider the performance trade-offs that varied with how thermally isolated or thermally conductive the sensor plate was. This condition is dependent on the leg length, as thermal resistivity is directly proportional the to resistance length.

$$R=\rho L/A \qquad [3]$$

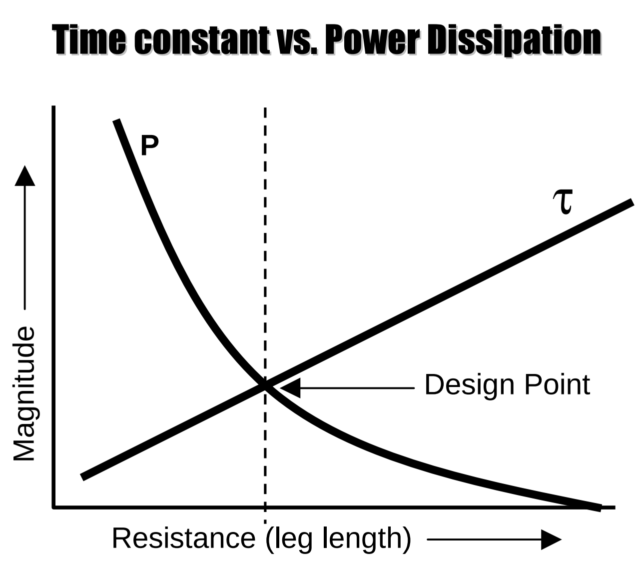

Figure 2: Qualitative plot showing how thermal *conductivity* (short legs) favors the time constant, τ, whereas thermal *isolation* (long legs) favors the power dissipation, P. It is desirable to choose a design to keep both values at a minimum.

The design specifications necessitated a time constant, τ, equal to 1 millisecond while keeping power dissipation, P, to a minimum. This represents a challenge, for if the plate is designed to be thermally isolated (long leg length), the power dissipation becomes ideal, however the sensitivity, or time constant, becomes dominantly worse. Yet if the device is designed to conduct heat away from the plate quickly (short leg length) to maintain an ideal time constant, the power dissipation becomes dominantly worse. This trend is depicted in Figure 2, and explained by the following two equations:

$$P = \Delta T / R \qquad [4]$$

$$\tau = R \times C \qquad [5]$$

Therefore, for a fixed capacitance, C, and change in temperature, ΔT, the power dissipation, P, goes like the inverse of the resistance, while the time constant, τ, increases linearly with resistance.

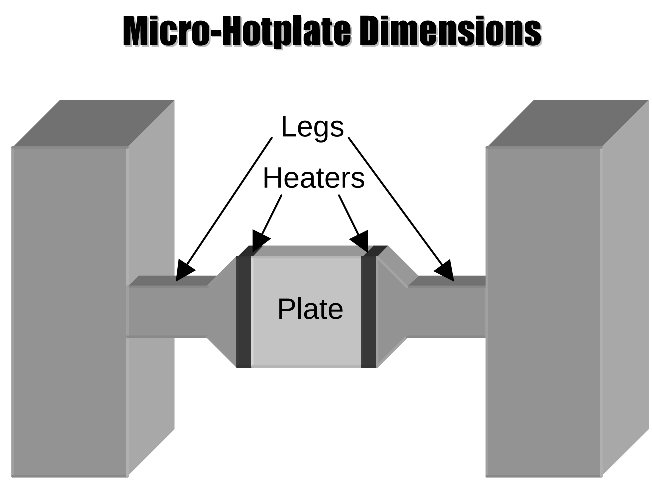

Figure 3: The hotplate device has an overall thickness of 3.5µm (there is an additional 0.1µm of platinum on the plate surface). The plate area is 80 × 80µm; each heater has an area of 4 × 80µm; the legs are 80µm long (heater to substrate) and 40µm wide with a 45° taper connecting to the heater.

Consequently, a design point was chosen which suitably satisfied the specifications. This fixed the leg length to be 80µm long. The overall structural dimensions are summarized in Figure 3.

STRUCTURAL ANALYSIS

Having set the overall dimensions of the micro-hotplate, it became critical to determine if the device would be structurally sound enough to resist buckling upon heating up to 400°C (for the micro-CVD reaction). If bucking proved to be a substantial concern, then the legs would need to be bent 90° to better allow for the expansion of the plate; however this would compromise the ability to model the heat transfer of the system one-dimensionally.

Fixed-Fixed Beam Buckling

Euler's Buckling Criterion:

$k = 2\pi/L$ $F_{crit} = E\,I\,k^2$ $\sigma_{buckling} = F_{crit}/A$

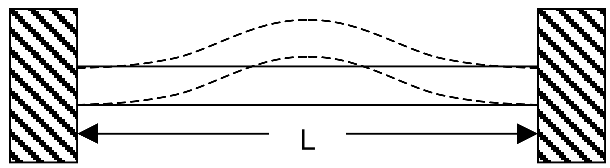

$\sigma_{thermal} = E\,\alpha\,\Delta T\,L_{plate}/L_{total}$

Figure 4: If the stress caused by thermal expansion within the beam, $\sigma_{thermal}$, is greater than the allowable buckling stress across the beam, $\sigma_{buckling}$, the beam will *buckle.*

First order calculations were carried out modeling the device as a straight, fixed-fixed beam of constant width 40μm (see Figure 4). The stress across the beam was assumed to be generated solely from the expansion of the plate (since the temperature drops off quickly across the heaters and legs). This yielded the following equation[1]:

$$\sigma_{thermal} = E\,\alpha\,\Delta T\,L_{plate}/L_{total} \qquad [6]$$

Where E is the composite modulus of elasticity (~107 GPa), as determined by Rule of Mixtures for composite beams in axial loading (essentially a volume weighted average)[10]. The composite coefficient of thermal expansion, α, was calculated to be ~1.35μm/m°C. And the ΔT is the temperature increase from room temperature to 400°C (~375°C). This yielded a stress due to thermal expansion, $\sigma_{thermal}$, to be approximately 17 MPa.

Now, using the Euler Buckling Criterion for this configuration, as outlined in Ashby[11], a foundation stiffness, k, is calculated,

$$k=2\pi/L, \qquad [7]$$

where L is the overall length of the beam (L=248μm). The critical force at which point buckling occurs is dependent on the composite modulus of elasticity, E, the moment of inertia of the beam, I, and the foundation stiffness, k:

$$F_{crit} = E\,I\,k^2 \qquad [8]$$

Dividing this force by the cross-sectional area, A, yields a maximum stress before buckling, $\sigma_{buckling}$, equal to approximately 70 MPa. This calculation ignores the fact that the beam widens to 80μm for a significant portion in the center, which would presumably increase the moment of inertia, increasing the buckling stress to over 100MPa. In either case, the thermal stress ($\sigma_{thermal}$ = 17 MPa) is a significantly lower value ($\sigma_{buckling} > \sigma_{thermal}$), so to first order the device should not buckle. Therefore the legs should not have to be designed any differently, and the treatment of the heat transfer modeling as a 1-D system is a valid assumption.

For this structural analysis to be more valid, it is important to note that residual stress in the fabricated device may dramatically alter the bucking conditions. Thermal oxide, which accounts for 1μm of the beam thickness is usually in residual compression from 200-300

MPa[12]. However, CVD oxide, which accounts for 1.4μm of the thickness is typically in residual tension of about 100-400 MPa[13]. Due to this wide variability in residual stress, it was opted to neglect this issue from the first order calculations.

CHEMICAL VAPOR DEPOSITION

For our Pt CVD we have several known precursors to choose from. These include $Pt(CO)_2Cl_2$, Pt acetylacetonate and $Pt(PF_3)_4$.[14] Platinum acetylacetonate precursors cause heavy carbon contamination. The $Pt(CO)_2Cl_2$ precursor produces nearly pure films, but they exhibit poor adhesion.[15] Finally, the Pt trifluorophosphine complex yields good results and was used by a group at the University Of Michigan for a gas microsensor application, thus we chose $Pt(PF_3)_4$ as our LPCVD precursor.[16]

The platinum deposition is a surface reaction. We can use an order of magnitude estimate to determine if our reaction chamber concentration is uniform. In this case, we use the Peclet number (Pe) which relates convection to diffusion. For Pe >> 1, our CVD chamber is not well mixed and bulk transport issues are important. For Pe<< 1,then our chamber is well mixed. For our CVD process our pressure is extremely low so based on our Peclet number shown in Eq. 8, we can conclude that our reaction zone is well mixed during our deposition because of the high diffusivity at low pressure.

$$Pe = \frac{uL}{D} \qquad [9]$$

where u = velocity
L = characteristic length
D = diffusivity.

When considering a smaller window at the substrate surface where we consider molecular transport and we have no slip and no penetration boundary conditions so that u = 0, a surface reaction may be regarded as occurring in five consecutive steps as follows:

Diffusion of the reactant molecules to the surface.
Adsorption of the gases on the surface.
Reaction on the surface.
Desorption of the products.
Diffusion of the desorbed products into the main body of the gas.

At one time it was believed that one of the diffusion processes, 1 or 5, was the slowest process and therefore determined the overall rate. More detailed investigations of surface reactions showed that this could not be the case. This is evident from the fact that heterogeneous processes nearly always involve appreciable activation energies, whereas diffusion in the gaseous state involves no activation energy; the diffusion process therefore is much more rapid than the overall process and cannot constitute its slow step.[17]

We are given an assumed rate of change in height of the Pt film as a function of temperature. The actual thickness is found by determining the temperature at a node as a function of time and inserting it into the Arrhenius expression. Then we can integrate that expression with respect to time to determine the thickness at a point. If we assume that the deposition, whether it is exothermic or endothermic, does not change the temperature profile of the plate, then we can simply take the height of the film as the product of the Arrhenius expression and the deposition time.

FABRICATION

As stated earlier, the microhotplate must fabricated in a standard CMOS process flow, with the structure release happening in a back-end micromachining step. This section describes the process flow, process parameters, and mask layouts.

CMOS Process

The CMOS process used here is part of a multi-user foundry service called MOSIS (www.mosis.org). MOSIS supports many different fabrication processes, currently ranging from a 2.0 μm (minimum) feature size with 2 layers of metal to a 0.35 μm feature size with 4 layers of metal. In addition, MOSIS supports mixed-signal and analog product lines, as well as GaAs processes.

The first step in using MOSIS is to choose the process technology. Although it would be desirable to use the most aggressive process (in terms of linewidth and number of interconnect layers), the microhotplate is a relatively gross device which does not require these features. In addition, these more aggressive processes are more expensive, increasing the overall cost of the device.

Because of these reasons, we have chosen to use the least aggressive MOSIS CMOS process, which is the 2 μm n-well CMOS process. This is a double-poly, double-metal process administered by Orbit Semiconductor. While many process specifications are proprietary, the following with relevance to our design were successfully obtained:

Table 2: Orbit Semiconductor 2 μm Process Specifications

Parameter	Value	Reference
Gate oxide thickness	400 Å	http://www.orbitsemi.com/cmos_2n.html
Field oxide thickness	1 μm	personal communication with ginger wang
CVD oxide 1 thickness	0.06 μm	http://www.orbitsemi.com/cmos_2n.html
CVD oxide 2 thickness	0.6 μm	personal communication with ginger wang
CVD oxide 3 thickness	0.5 μm	assumed
CVD oxide 4 (overglass) thickness	0.1 μm	assumed
Poly 1 thickness	0.5 μm	personal communication with ginger wang
Poly 2 thickness	0.5 μm	assumed
Poly 1 & 2 sheet resistance	21 - 25 Ω/sq	http://www.orbitsemi.com/cmos_2n.html

The overall fabrication process is a standard LOCOS (local oxidation of silicon) n-well process, as described in ,[18] with the addition of a second polysilicon layer above the first one, and with two layers of metal instead of one. In addition, MOSIS makes a concerted effort to allow for post-CMOS micro-machining, by including two tiles specific to MEMS structures. Both tiles were initially included to allow for anisotropic wet etching of Si in EDP (ethylenediamine pyrocatechol) .[19] The first tile is for a heavily-doped etch-stop layer which is not necessary for our process. The second tile is called the 'open' tile, and it is used to make openings to the silicon substrate for post-CMOS micromachining. MOSIS takes the layout of the open tile and expands into to the necessary etch masks to ensure that at the completion of the process that the silicon surface will be exposed. The rules for using the open tile, along with background about MEMS support from MOSIS can be found in [19]. In addition, the layout rules for the 2 μm Orbit process can be found in [[20]].

Process Flow

The process flow starts with p-type silicon wafers. The first step in the process is to form the n-wells. Since we have no n-wells in our process, we have a blank mask for this step. After the n-wells are defined, a thin oxide is grown and a nitride layer is deposited on top. These are patterned and etched to form the active area. This mask is part of the open tile. The next step is to implant the channel stop layer, and again we have a blank mask for this step.

The next step in the process is the growth of the thermal field oxide. This oxide is grown everywhere that the silicon isn't covered with nitride, and is thus a maskless way to form the field oxide, dubbed the LOCOS method (Figure 5a). After the field oxide has been grown, the masking nitride and thin oxide are stripped. The gate oxide is grown next, growing everywhere that the field oxide is missing (Figure 5b). Following this, the first layer of polysilicon is deposited (Figure 5c). It is patterned to form our sense resistor. The applicable design rules for this layer are:

Table 3 Poly 1 (Sense Resistor) Design Rules

Minimum linewidth	2 μm
Minimum spacing	2 μm
Minimum spacing from edge	2 μm

After the polysilicon is patterned, it is doped with phosphorous in the same step as the source/drain regions are made. Since it does not matter if the whole wafer is doped n+, we have an open mask for this layer. A p+ implant comes next, to define the p+ areas on the wafer. Since we do not have any of these, we do not have any features on this mask.

After the first layer of poly is finished, an interpoly oxide is deposited and patterned with the same features as the open layer. Then the second layer of poly is deposited, patterned, and doped (it is not clear if this layer is in-situ doped or implanted) (Figure 5d). This layer will form the heater resistor. The design rules for this layer are:

Table 4: Poly 2 (Heater Resistor) Design Rules

Minimum linewidth	3 μm
Minimum spacing	3 μm
Minimum spacing from edge	3 μm

Following the second layer of poly, the backside processing continues with the depostion of another CVD oxide dielectric spacer between poly 2 and the first layer of metal. This layer is the first contact layer and is patterned to form contacts between metal 1 and the two poly layers. The applicable design rules for this layer are:

Table 5: Contact Layer Design Rules

Via Size	2 μm x 2 μm

The first layer of metal is then deposited and patterned (Figure 5e), followed by a third CVD oxide to serve as the interlevel dielectric between metal 1 and metal 2. This oxide is the via layer and has the same design rules as the contact layer. Next, the second layer of metal is deposited and patterned. Since we are not using this second layer of metal, it is completely etched off the surface of the wafer. Finally, the overglass passivation layer (CVD oxide 4) is deposited and holes are patterned that to allow for contact to the metal 1 layer (Figure 5f). This completes the CMOS fabrication process.

Post-CMOS Fabrication

Following CMOS fabrication, the microhotplate must be released from the substrate in order to thermally isolate it. Several methods exist to etch the structure, and they can be broadly classified into two regimes - wet etches and dry etches. Wet etches consist of etchants that anisotropically etch silicon with very high selectivity to oxide and which will not harm the aluminum metal layers. The most common etchant for this is EDP, which is the etchant initially proposed by MOSIS. The problem with wet etchants are two-fold. First, compliant MEMS structures with very small gaps may end up sticking together during the drying process, as the water tension pulls them together. This problem of stiction is a concern for some structures, but is not an issue with the microhotplate because the gaps are relatively large. A second problem with wet etchants is that the rinsing and drying process can be quite violent. This can cause fragile structures (such as the microhotplate) to break, leading to yield problems.

To avoid the rinsing and drying, we have chosen to use dry isotropic silicon etchant xenon diflouride (XeF_2). This etchant is a white solid which sublimates at room temperature to form the gas form, which readily reacts and etches silicon [21]. The etchant requires no external energy source, such as heat or a plasma, to etch. In addition, xenon diflouride has virtually infinite selectivity to the other exposed materials, namely aluminum and silicon dioxide. The drawback with using xenon diflouride is that the isotropic nature of the etch means that undercutting of the silicon substrate will occur, increasing die size.

The actual etch would be done by placing the sample in the etching chamber and pulsing the gas over the substrate. The etch rate can vary, but a nominal etch rate of 5 - 8 μm/min could be used to initially time the etch [21]. Test structures such as a microhotplate with no legs, which would blow away when released, could be used to determine the release time. The amount of overetch time (after release) necessary to completely remove the silicon from the microhotplate would probably be determine experimentally by destructive visualization of the microhotplate undersides.

The final structure and cross section is shown in Figure 5f.

The final structure and cross section is shown in Figure 5f.

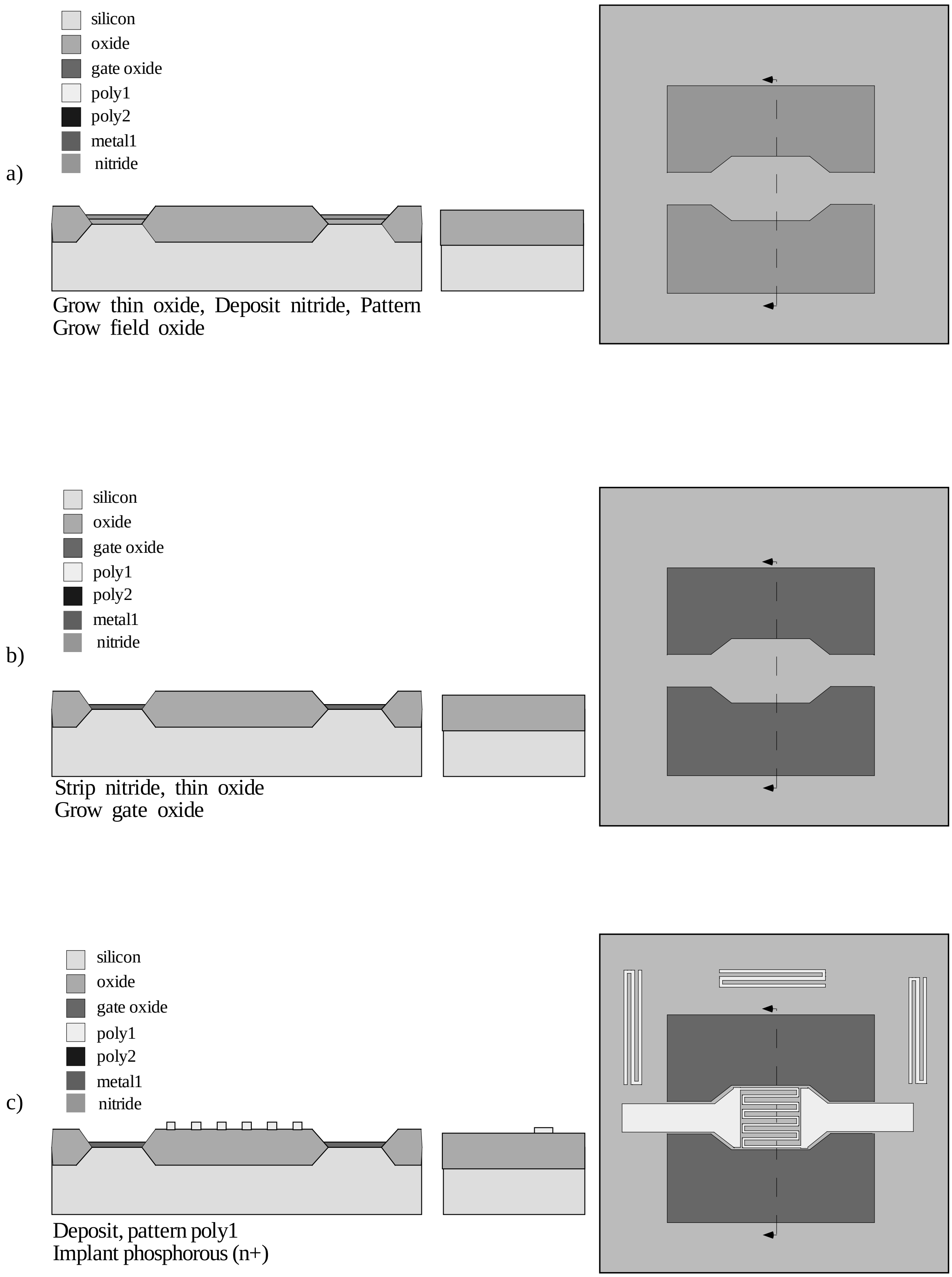

Figure 5a-c. CMOS Fabrication process.

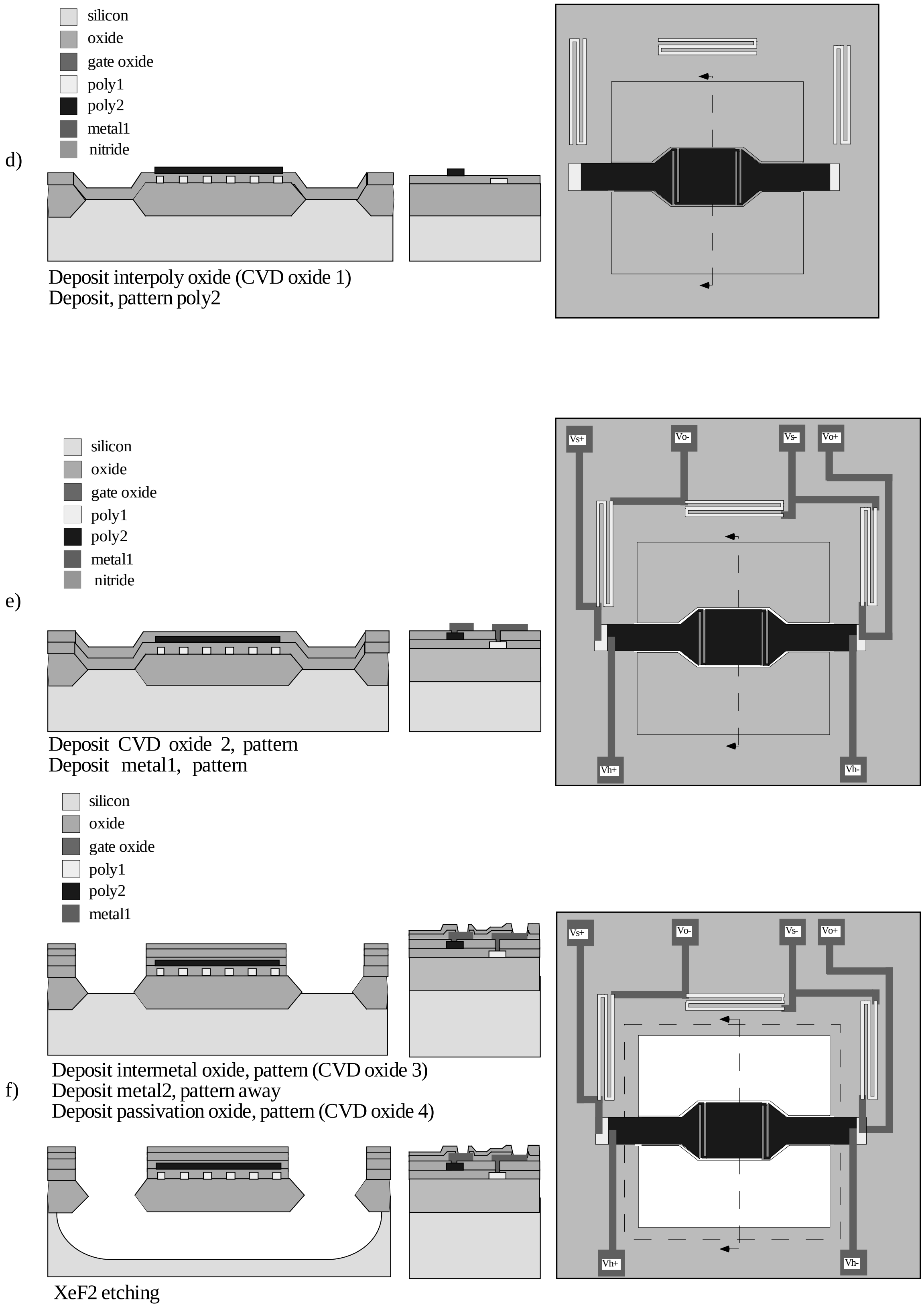

Figure5d-f. CMOS Fabrication process, cont.

ELECTRICAL CHARACTERISTICS

There are several electrical parameters that need to be determined to adequately characterize the microhotplate. Some, like the polysilicon layer sheet resistances, are given, but others must be determined. These include the temperature coefficient of resistance (TCR) of the polysilicon heater and sensor and the noise characteristics of the system.

TCR of Polysilicon

In order to design the polysilicon resistors, both for sensing and heating, we need to know the resistivity of the material at elevated temperatures. The relationship of the high-temperature resistivity of the material to the room-temperature resistivity is given by the following relation:

$$\begin{aligned} R(T) &= R(T_0) + \Delta R \\ &= R_0(1 + TCR \cdot \Delta T) \end{aligned} \qquad [10]$$

This relationship assumes that the TCR of the material is constant over the temperature range of interest. In actuality, the TCR will be a function of temperature, leading to a nonlinear dependence of the resistivity on temperature. In order to characterize the material, then, we must first determine the TCR and then determine over what temperature range it is valid.

Since polysilicon is an important electrical material, it has been well characterized over the temperature regimes where electronics operate (roughly 0-200 ˚C). Of particular relevance here is the behavior of heavily-phosphorous-doped polysilicon thin films, such as the ones used for gate electrodes on MOSFETs, which are the ones used here [22]. In addition, the theory of electrical transport in polysilicon thin films if well developed, and one could envision computing the TCR as a function of known deposition parameters [23].

The problem with the computational approach and with extracting the number from published reports is that the electrical properties of polysilicon are heavily dependent on processing parameters. Since we do not know all the processing parameters for the MOSIS films, it would be imprudent to select the TCR from a journal paper. Luckily, there exists a journal paper describing the TCR of polysilicon thin films deposited in a 2 μm MOSIS process [24], which is most probably the actual process that we are employing. The TCR listed in the paper is 0.001 $˚C^{-1}$, measured over the temperature range from 20-200 ˚C. In order to use this value for our TCR, though, we must determine whether it is applicable at 300 ˚C.

At a high enough temperature, the resistivity of polysilicon will exhibit nonlinear characteristics. We must determine this temperature limit. Since most conventional electronics never encounter the high temperatures that we are operating at, there have not been many studies on the TCR of polysilicon at these temperatures. One study which did deal with such issues was concerned with using polysilicon for the thermal assembly of microstructures, and thus the high-temperature properties (up to melting point) of polysilicon were crucial to the study [25]. The author observed that he could fit his resistance vs. temperature data to a model in which the resistivity of polysilicon was linear with temperature up to 600 ˚C. Since the polysilicon used in these experiments was similar to the polysilicon used here (heavily-doped n-type), we have assumed that a TCR of .001 $˚C^{-1}$ does indeed hold up to our operating temperature of 300 ˚C.

Noise

The minimum resolvable temperature change of our device, which determines our minimum detectable hydrocarbon concentration, is dependent upon the noise properties of the device and the measurement system. Order-of-magnitude estimations can easily be made by considering some relevant sources of noise.

Radiation Noise

Radiation noise is the thermal dissipative noise associated the exchange of heat between the microhotplate and the ambient [26]. It is always present in any system, with the limiting factor being dissipation via blackbody radiation only. It is a white noise source, and its magnitude is given by

$$\Delta P_{noise,R} = \sqrt{\frac{4kT^2\Delta f}{R_{th}}} \qquad \textbf{[11]}$$

where $\Delta p_{noise,\ R}$ is the average power in watts, T is the temperature of the system, k is boltzmann's constant, R_{th} is the thermal resistance connecting the system to ambient, and Δf is the measurement bandwidth. Using our values for R_{th} and T, and using a measurement bandwidth of 1 kHz, the equivalent power is

$\Delta p_{noise,\ R}$ = ~ 1 nW

Converting this noise power into a noise temperature via the leg resistances, we get a noise temperature of

$$\Delta\tau_{\nu o\iota\sigma\varepsilon,\ P} = \text{~}3\ \mu K$$

Johnson Noise in Resistors

The polysilicon sense and heater resistors will exhibit both exhibit Johnson noise. Since the heater resistance is approximately ten times less than the sense resistance, its noise component is neglected. Therefore, the Johnson noise term is given by

$$\Delta V_{noise,J} = \sqrt{4kTR_e\Delta f} \qquad \textbf{[12]}$$

where R_e is the electrical resistance of the sense resistors. Using the microhotplate values for these parameters (and a 1 kHz bandwidth), the Johnson noise is

$$\Delta v_{noise,\ J} = \text{~ } 1\ \mu V$$

Using the transfer function between output voltage of the wheatstone bridge and temperature on the hotplate, the equivalent temperature noise is

$$\Delta T_{noise,\ J} = \text{~}1\ mK$$

This is still quite small, even at 300 ˚C, because the sense resistors are of relatively low impedance (~25 kΩ @ 300 ˚C). This analysis does neglect other potential noise sources in these polysilicon thin-film resistors, such as shot noise between grains and surface recombination noise. These may increase the noise temperature somewhat.

Amplifier Noise

The amplifier used in the control circuit will introduce noise into the system. The amount of noise is very dependent on the particular amplifier chosen, but an estimate can be made by consulting off-the-shelf component specification sheets. Using an Analog Devices AD546 instrumentation amplifier as the input stage being driven by the output of the bridge, and assuming a 1 kHz bandwidth, the input noise of the amplifier is given as

$$\Delta v_{noise,\ A} = \text{~}10\ \mu V$$

The equivalent temperature noise for this is

$$\Delta T_{noise,\ A} = \text{~}10\ mK$$

Thus, the amplifier noise dominates, and the minimum resolvable temperature difference will be approximately 0.01 K, which is within specifications.

Thermal Modeling and Controls

In order to test the validity of our planned hot plate and to visualize the results of the temperature distribution over the whole structure, we create a numerical model based on the finite-difference approximation[27]. This is model is based on several simplifying assumptions:

1. Lumped-Capacity Analysis (the temperature is uniform in the thickness of the plate.)
2. One Dimensional Heat-Transfer.
3. Symmetric along the two major axis (Possible to use less nodes in the numerical formulation.)
4. Boundary conditions remain fixed at ambient temperature.

The first assumption establishes that the temperature in the direction of the plate thickness is uniform. This is commonly called the “fin-approximation” or “fin-assumption”. In order for this assumption to hold then the Biot number must be very small. The dimensionless group called the Biot number is defined as:

$$Bi = \frac{h(V/A)}{k} = \frac{hs}{k}$$

Where k is the thermal conductivity of the solid and h is the convection coefficient. The ratio V/A=s is a characteristic dimension of the solid.

A good rule of thumb for using lumped-capacity analysis is if Bi < 0.1. An order of magnitude estimation of Bi gives favorable results for using this analysis.

k ~ 2500 W/mK
h ~ 1 W/m^2K (for free convection)
h ~ 10 W/m^2K (for forced convection)
s ~ 100 μm

Even using the worst case for convection, lumped-capacity analysis is an appropriate approximation.

As a follow up to the fin approximation, which implies that conduction is the dominant form of heat transfer, we assume one dimensional heat transfer. Since, convection and radiation account for less than 0.5% of the total heat transfer, they are eliminated from the analysis.

One of the early designs of the hot plate had it as a fixed-fixed beam with uniform cross section along the entire length. Unfortunately, this gave too much area for heat conduction out of the hot plate region. Consequently, in order to maintain the hot plate at a steady-state temperature of 300 C, the power dissipation became exorbitant. Therefore, the plate needed to be more thermally isolated which was accomplished by reducing the leg width.

As a result of reducing the leg width the fixed-fixed beam no longer had a uniform cross section along its entire length. By making a sudden transition in dimension between the plate and the legs, one dimensional heat flow would be a poor model. However, by putting a transition region in the legs the one dimensional model becomes a better approximation.

The final assumption that needs explanation is that our hotplate is symmetric. Therefore, when implementing the finite-difference approximation we need only solve half of the hotplate in the one-dimensional case and a quarter of the hotplate in the two-dimensional case. A two dimensional model was never completed but would be advised before actual construction.

A steady state and an unsteady-state model were implemented to solve the temperature distribution in the hotplate. For the steady state model the equation:

$$q_i + \sum_j \frac{T_j - T_i}{R_{ij}} = 0$$

Solves the temperature distribution. T is the temperature at each node, R is the thermal resistance between nodes, and q is the heat generated a node. R is dependent upon the characteristics of the material, the respective amounts of material, and the size of the nodes. Since the minimum line width of the processing was 2 microns, each node was set to be 4 microns.

The finite difference can also be written matrix form:

$$R\vec{T} = \vec{q}$$

In the one-d case, R is a tridiagonal matrix and T can be solved very easily and quickly in Matlab.

The figure shows the solution for the steady-state temperature profile for the hot plate. The hotplate outline at the top of the plot is shown for clarity in understanding what part of the plate is at what temperature.

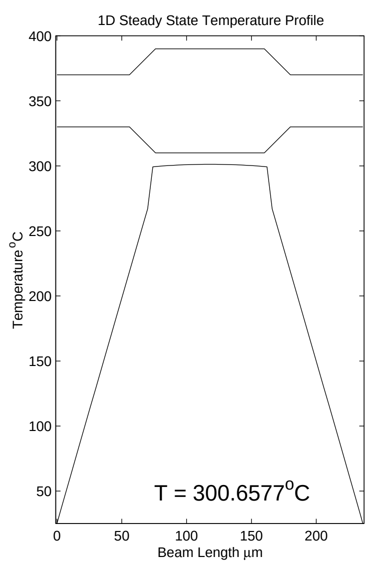

Notice the uniform temperature across the plate. There is a slight variation across the plate as a result of the heat dissipation in the sense resistor. The heat generated by the heaters causes a sharp temperature rise. This helps thermally isolate the plate. These results indicate that the model behaves as expected.

The actual hotplate will be used as a dynamic system. In order to explore the dynamics of the system, an unsteady state model is created. Using the forward difference method similar to the steady-state model derivation we find an explicit relation for temperature as a function of time. For this equation C is the thermal capacitance for each node and the superscript p+1 denotes the temperature at the next time step. The time step duration is constrained by the following relation to insure stability:

$$T_i^{p+1} = \frac{\Delta\tau}{C_i}\left[q_i + \sum_j \frac{T_j^p - T_i^p}{R_{ij}}\right] + T_i^p$$

$$\Delta\tau \leq \left[\frac{C_i}{\sum_j (1/R_{ij})} \right]_{\min}$$

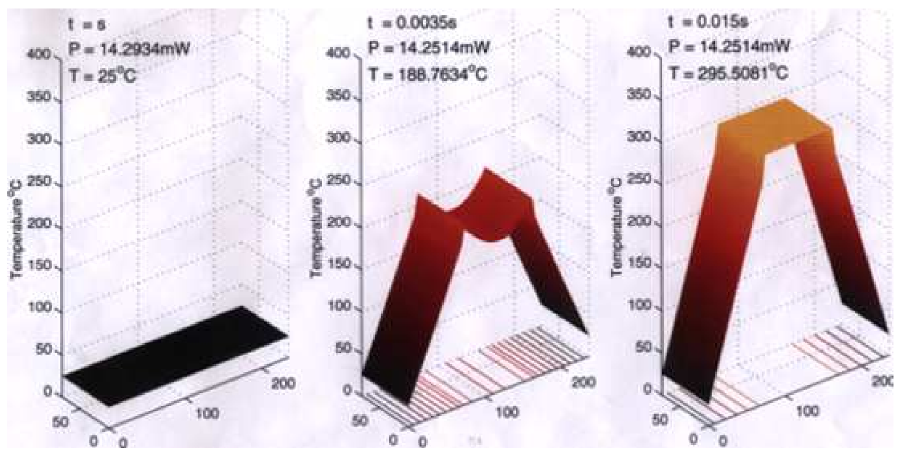

Figure 6: Open Loop Response

For the one-d model used in this report the minimum required time step was 1.9 μs but we used 1.0 μs just to guarantee stability and to make understandable time steps.

The plot shows three steps in time to have the system go from ambient temperature to its operating conditions under a constant power input. It took over 15 ms to reach steady state. Using lumped parameters we found the time constant to be on the order of 3 ms +. At 3.5 ms you can see that the system has reached ~63% of its steady-state operating temperature. At 15 ms it has reached ~98% of final. This indicates that the lumped parameters are at least in the right ball park.

Control

The specification was to have the time constant be 1 ms. By applying feedback control on the plate we can gain a 1 ms time constant. Open loop, the system is first order with

$$\frac{T}{q} = \frac{K}{\tau s + 1}$$

We could simply use a proportional controller to increase the time constant but that would yield a steady state offset error from the desired temperature. Therefore, to eliminate the error, we use a PI controller and increase the gain to reach the 1 ms time constant. The root locus for the controlled system is shown here:

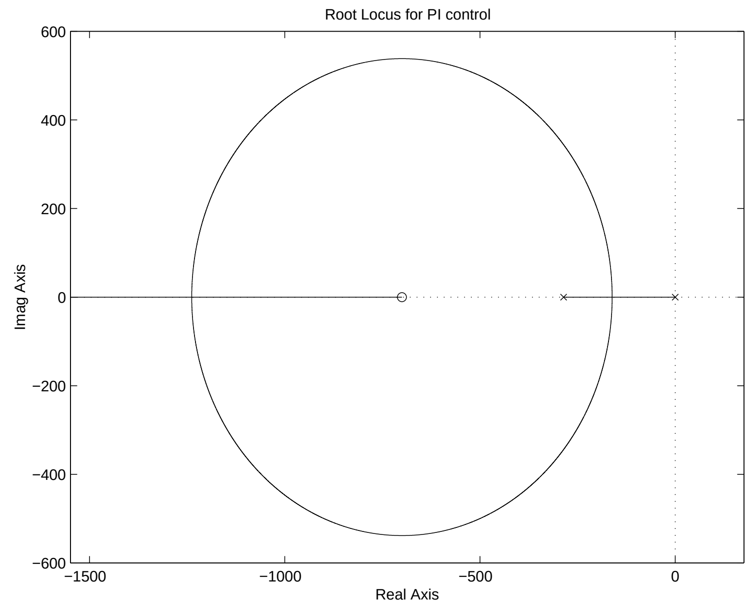

The next picture shows six time steps of the closed controller bring the system to operating temperatures. With this controller there is significant overshoot as seen at 1 ms but by 4 ms steady state has been reached.

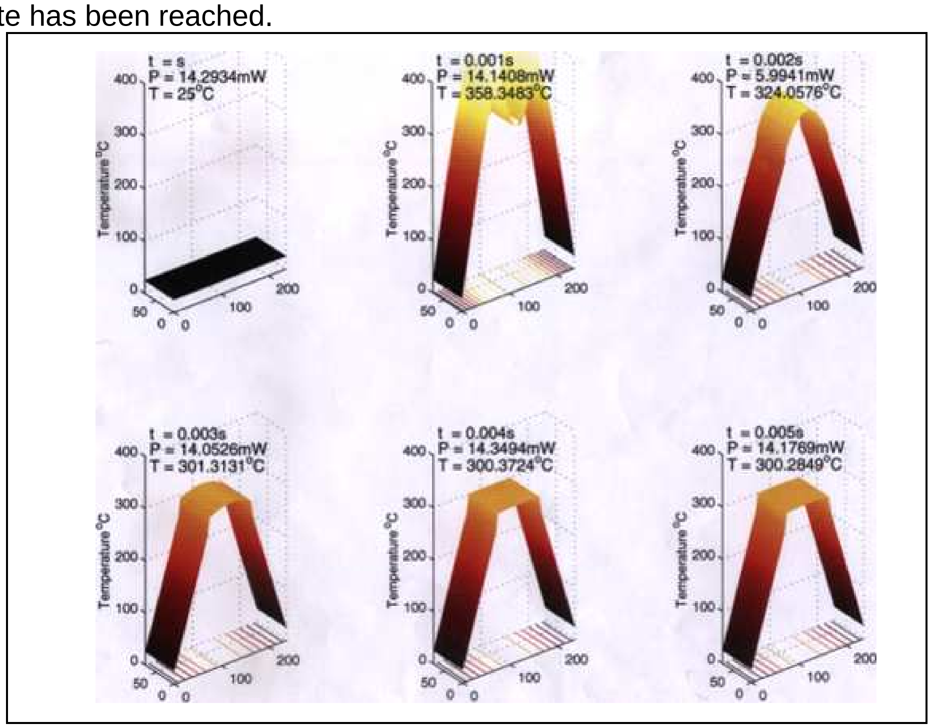

Figure 7: Closed Loop Unlimited Power

Unfortunately, this is an unrealistic controller. In order to get such a quick rise time, an incredible amount of power must be generated by the heaters. The amount of power is far outside the limits of our amplifier. So, to get some insight as to how the hotplate will respond with limited power, we placed a power limit in the simulation. The system still responds very well but the rise time is slowed dramatically because of the slew limit of the amplifier. In reality, the power limit would not be a simple limit but is actually a function of temperature. But this simulation at least gave us a sense of what would happen. It must be mentioned that during operation, the temperature of the hotplate only changes a small amount and does not make the jump from room temperature to operation very often.

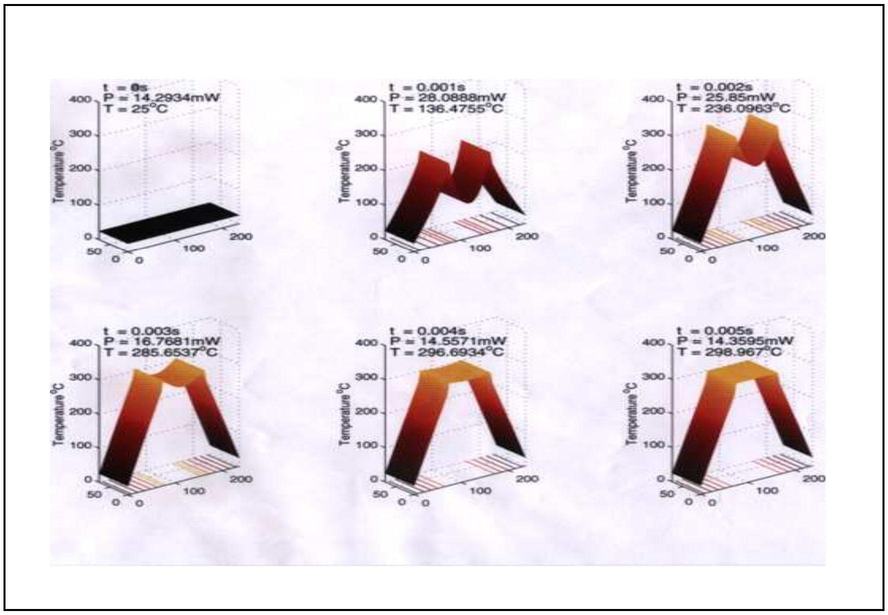

Figure 8: Closed Loop Unlimited Power

Steady state operation.

Finally, we want to see what happens during steady state operation as hydrocarbons react with the platinum catalyst. As mentioned before, the deposition of platinum on the plate is basically limited to the plate area only. Therefore, the heat of reaction will only occur on the plate itself. In simulation, this is done by adding heat to each node over the plate at specified times. The simulation shown in the figure has reactions starting at 1 ms and stopping at 4 ms.

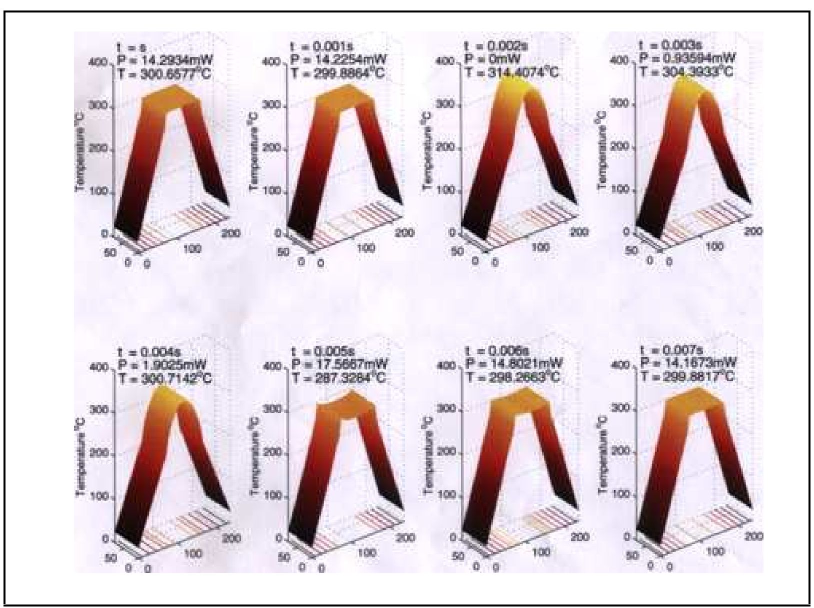

Figure 9: Simulation of HC's Reacting on the Plate

There are three are two points of interest in the simulation. You can see that there is a parabolic temperature distribution over the plate while there is heat from the reaction. This is a good demonstration why it is a bad idea to have a heater distributed over the entire hotplate area. Heat flows only when there is a temperature gradient. So, if heat is generated in the middle of the plate then it will force a non-uniform temperature distribution over the plate. This would have bad results on the deposition of platinum during the microCVD. The other point is that the heater is limited in both directions. The heater can only turn on so much and just as important can only turn off (i.e. The heater cannot remove heat.) An example of this is seen in the third frame as the controller tries to make the hotplate come to an average temperature of 300 degrees. The power into the heater is 0 W. Regardless of being power limited, the hotplate still responds very quickly.

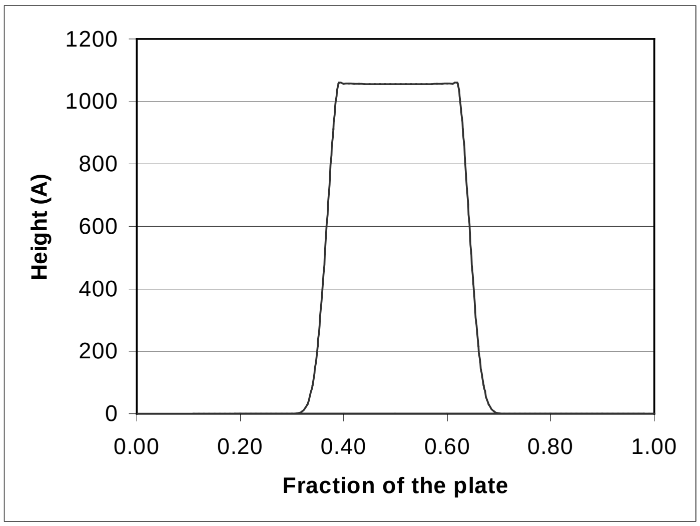

Figure 10: Platinum Profile

Using our thermal model, we estimated our Pt catalyst film profile. The slight non-uniformity in the Pt region is a result of the platform being slightly hotter near the heaters.

SENSOR PERFORMANCE

As stated, our sensor is used to detect combustible gases. Our design is not sensitive to various combustible gases based on the detection method. Alternatives to incorporate sensitivity include using an array of sensors with catalysts that respond differently to various hydrocarbons to increase sensitivity or perhaps obtain sensitivity by using the multidimensional information contained in a dynamic non-linear response.[28] For our performance evaluation we only consider hydrocarbons, although gases other than hydrocarbons, such as ethers, are combustible. Furthermore, we examined the heat of combustion for straight chain parrafins (n-alkanes) in comparison to other hydrocarbons. We show a plot of the heat of combustion vs.

the number of carbons for parrafins. The relationship is clearly linear. In addition to the plot of n-alkanes, we include a plot of n-alkanes and other hydrocarbons such as iso-parafins and alkenes to compare the heats of combustion. As seen, the relationship is still linear although there is error introduced.

To determine our operating range, we assume that the HC we are sensing in octane. Our upper operating boundary is determined by our ability to dose the sensor. For a given power, our sensor is saturated once all the power is supplied by the reaction. For that power we can determine the corresponding molar flow rate assuming all the heat from the reaction is transferred to the plate. Also, we assume that we have a total hydrocarbon conversion. Once we know the flow rate, using the ideal gas assumption we can determine the corresponding volumetric flow rate. We assume that we can dose the sensor accurately at no less that 5 sccm. Using these assumptions and assuming 5 mW power consumption, our upper sensing boundary is 280 ppm. Our lower sensing boundary is determined by our temperature resolution. Assuming the .5 °C specification, the overall heat transfer coefficient $U \neq f(T)$ and that there is a linear relationship between temperature and power, we can determine our lower operating boundary. Assuming a 5mW power consumption over the 25°C to 400°C range, our slope is $1.3 * 10^{-6}$ W/°C. For a .5C resolution, the corresponding sensor boundary assuming the gas is ideal and the HC is octane is <1 ppm.

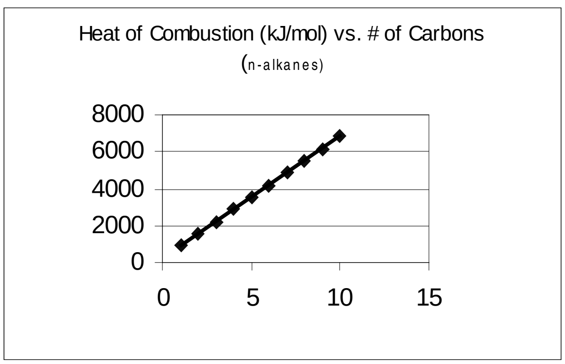

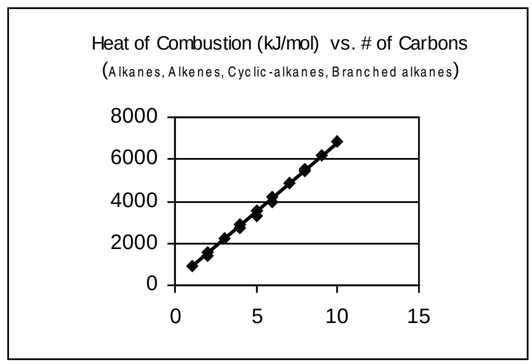

Figure 11: Heats of Combustion for Hydrocarbons

CONCLUSIONS

We have designed a combustible gas sensor. Buckling is an issue. The Pt deposited by LPCVD for the catalyst is uniform. We can adhere to CMOS processing constraints and still obtain a feasible device. With a PI controller, we operate with a 1 ms time constant at 14 mW of power. Our sensor operates in the range of 1 to ~300 ppm.

REFERENCES

[1] M. J. Madou, S. R. Morrison, *Chemical Sensing with Solid State Devices*: Boston, Academic Press, Inc., 1989, pp. 13-44.

[2] M. J. Madou, S. R. Morrison, *Chemical Sensing with Solid State Devices*: Boston, Academic Press, Inc., 1989, pg. 1.

[3] M. J. Madou, S. R. Morrison, *Chemical Sensing with Solid State Devices*: Boston, Academic Press, Inc., 1989, pg. 2.

[4] S. H. Phelps, *Effects of Variations in Sampling Pressure on the Response Time and Output of A High Speed Flame Ionization Detector,* B.S. Thesis, MIT Cambridge, MA, 1988. Pg. 7.

[5] B. A. Schaefer, "The Calculation of Ion Currents in Hydrocarbon Flames", *Combustion and Flame, 56:43-49(1984).*

[6] S. S. Zumdahl, *Chemistry,* 2nd ed., Lexington, MA: D.C. Heath and Co., 1989.

[7] M. J. Madou, S. R. Morrison, *Chemical Sensing with Solid State Devices*: Boston, Academic Press, Inc., 1989, pg. 2.

[8] C. N. Satterfield, *Heterogeneous Catalysis In Industrial Practice,* 2nd ed., New York: McGraw Hill, Inc., 1991. Pg. 26.

[9] S. L. Firebaugh, *Investigation of Materials for Use in High-Temperature, Thin-Film Heaters and Temperature Sensors,* M.S. Thesis, MIT, Cambridge, MA, 1997, Pg. 19.

[10] Callister, W.D., *Materials Science and Engineering*, John Wiley and Sons: New York, 1994, p217.
Insett

[11] Callister, W.D., *Materials Science and Engineering*, John Wiley and Sons: New York, 1994, p517.
Insert 2

[12] Ashby, M.F., *Materials Selection in Mechanical Design*, Butterworth Heinemann: Oxford, England, 1996, p263.
nsert 3

[13] Hu, S.M., "Stress-Related Problems in Silicon Technology", J. Appl. Phys., Vol. 70, No. 6, (1991).Insert 4

[14] M.J. Rand, "Chemical Vapor Deposition of Thin Film Platinum," *J. Electrochem. Soc.,* May '73 PP. 686-692.

[15] M.J. Cooke, "A Review of LPCVD Metallization for Semiconductor Devices," *Vacuum* , 35:2,67-73 (1985).

[16] S.J. Majoo, "A Silicon Micromachined Conductometric gas sensor With a Maskless Sensing Film Deposited by Selected-Area CVD, *Sensors and Actuators B 35-36(1996)312-319.*

[17] K.J. Laidler, *Chemical Kinetics,* 3rd ed., Harper Collins Publishers, Inc., 1987, Pg. 241.

[[18]] N. H. E. Weste, K. Eshraghian, *Principles of CMOS VLSI Design: A Systems Perspective*, Reading, MA: Addison-Wesley, 1993.

[[19]] V. Tyree, J-I. Pi, C. Pina, W. Hansford, J. Marshall, M. Gaitan, M. Zaghloul, D. Novotny, "Realizing suspended structures on chips manufactured by CMOS foundry processes through the MOSIS service," [Online document], Available FTP: ftp.mosis.org/pub/mosis/cell-libraries/nist-mems-1.doc.

[[20]] "MOSIS Scalable CMOS (SCMOS) Design Rules", Revision 7.2. Available FTP: ftp.mosis.org/pub/mosis/designrules/scmos-rules-rev72.ps.

[[21]] P. B. Chu, J. T. Chen, R. Yeh, G. Lin, J. C. P. Huang, B. A. Warneke, K. S. J. Pister, "Controlled pulse-etching with xenon diflouride," In*Transduers '97*, Chicago, 1997 pp. 665-668.

[[22]] M. J. Dean, A. A. Naem, L. Y. Chee, "Temperature effects on heavily doped polycrystalline silicon," *Journal of Applied Physics*, Vol. 76, No. 9, pp. 5253-5259, 1994.

[[23]] C-Y. Wu., W-D. Ken, "A new computer-aided simulation model for polycrystalline silicon film resistors," *Solid-State Electronics*, Vol. 26, No. 7, pp. 675-684, 1983.

[[24]] N. George, A. Srivastava, "Design, fabrication and testing of polysilicon microheaters in silicon," *SPIE*, Vol. 2880, pp. 224-230.

[[25]] G. K. Fedder, "Simulation of Microelectromechanical Systems," Ph. D. Thesis, University of California at Berkeley, 1994.

[[26]] R. W. Whatmore, "Pyroelectric devices and materials, "*Reports on Progress in Physics*, Vol. 49, pp. 1335-1386, 1986.

[27] Holman, J.P., "Heat Transfer", Seventh Edition, McGraw-Hill, San Francisco, 1990.

[28] S. Nakata,"Gas Sensing Based on a Nonlinear Response: Discrimination Between Hydrocarbons and Quantification of Individual Components in a Gas Mixture," *Analytical Chemistry 68(1996)2067-72.*